Chapter 10
Processing of Transparent Materials Using Laser-Induced High-Energy State in Liquid

Tadatake Sato

Abstract High-energy states formed upon focused laser irradiation are a basic phenomenon in laser material processing. The high-energy states formed in liquid can also contribute to material processing. When laser pulses are focused onto the solid–liquid interface through solid materials, a high-energy state is generated at the interface. More precisely, it is generated in a thin liquid layer in contact with solid materials. Laser-induced backside wet etching (LIBWE) is a laser micromachining technique that utilizes the action of such high-energy states at the solid–liquid interface. Precise micromachining of hard and brittle transparent materials was achieved using this technique. The simple concept of this technique allows a variety of combinations of lasers, materials, and experimental setups for processing. While the concept for processing is relatively simple, the mechanism of the material removal is rather complex and has not yet been fully elucidated. A variety of material combination and conditions of laser irradiation is a factor making it more complex. Several attempts have been made to address the action of the high-energy state in liquid for material removal. Studies regarding LIBWE are overviewed in the context of the action of high-energy state generated in liquid.

Keywords Laser processing · Micromachining · Transparent materials · Laser-induced backside wet etching (LIBWE) · Laser-absorbing liquid

10.1 Introduction: High-Energy States in Liquid for Laser Processing

The formation of local high-energy states upon focused irradiation of laser pulses is a basic phenomenon in processing of various materials with lasers [1]. Upon absorbing the energy of laser light, the irradiated part is instantaneously heated; thus, the formed local high-energy state results in the removal of materials by melting,

T. Sato (✉)
National Institute of Advanced Industrial Science and Technology (AIST), Tsukuba Central 2, 1-1-1 Umezono, Tsukuba 305-8568, Ibaraki, Japan
e-mail: sato-tadatake@aist.go.jp

© The Author(s), under exclusive license to Springer Nature Singapore Pte Ltd. 2022

Y. Ishikawa et al. (eds.), *High-Energy Chemistry and Processing in Liquids*,
https://doi.org/10.1007/978-981-16-7798-4_10

evaporation, or ablation. The recent development of high-power lasers with kW-classes has contributed to high-speed processing in the industry. Moreover, laser light can be focused into a small spot at the micrometer scale. Therefore, the precise micromachining of solid material surfaces is executable. This type of laser micro-processing can be applied to various materials ranging from hard materials such as metals and ceramics, to soft materials, such as organic materials and biological tissues.

Similar phenomena can be induced on the surfaces of liquids. Laser ablation from the liquid surface has been studied to obtain a better understanding of the mechanisms of laser ablation in more complex solid systems [2, 3]. Material ejection from the free surfaces of liquid has been observed similarly to solid materials when the fluence of the irradiation exceeds the threshold [4–6]. Laser ablation of liquid was investigated using a nanosecond imaging technique, as shown in Fig. 10.1. The threshold was evaluated at 100 mJ/cm^2 for benzene irradiated by ultraviolet (UV) pulses of a KrF excimer laser [4]. The difference in threshold values for several benzene derivatives was revealed to be correlated to the efficiency of photochemical bond dissociation [5]. On the other hand, the ablation of diluted solutions of benzene derivatives showing relatively larger thresholds was discussed based on the photothermal mechanism [6]. Thus, the high-energy states used in laser material processing can be formed on the surface of liquids. Note, laser ablation of laser-absorbing liquids should be distinguished from laser-induced breakdown in transparent liquids, which are often used

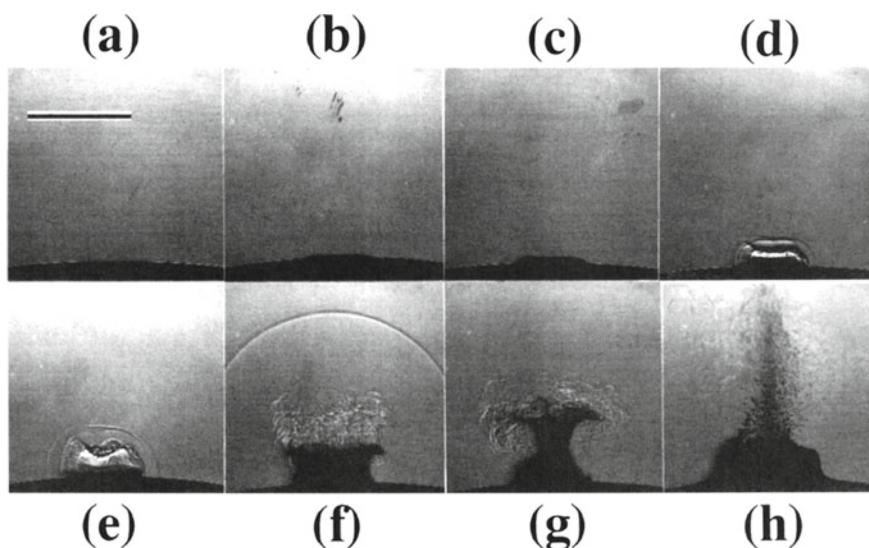

Fig. 10.1 Nanosecond images of laser ablation of liquid toluene. The scale bar represents 2 mm. Delay time: **a** 0 ns, **b** 35 ns, **c** 100 ns, **d** 500 ns, **e** 1 µs, **f** 5 µs, **g** 10 µs, and **h** 100 µs. Reprinted with permission from Ref [5], Copyright 1994 American Chemical Society

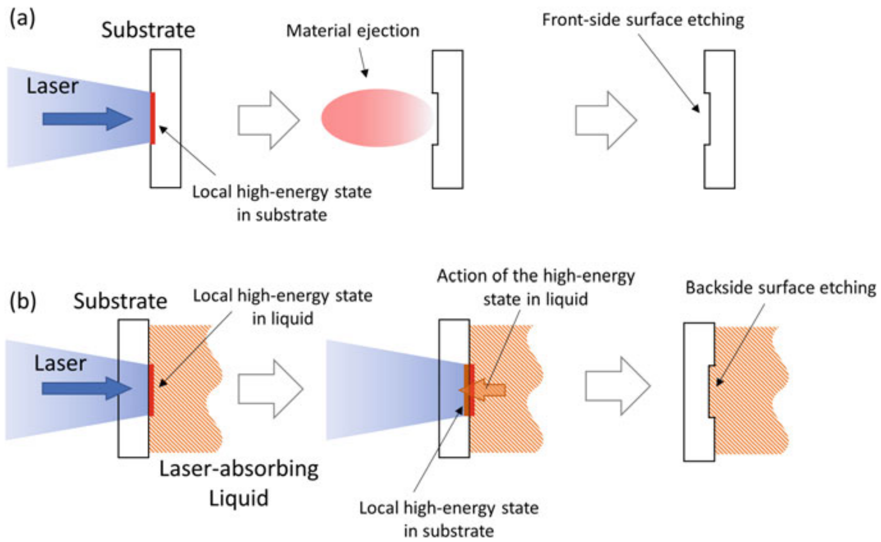

Fig. 10.2 Schematic drawing of **a** direct and **b** indirect laser processes

for laser-induced breakdown spectroscopy (LIBS) measurements for the elemental analysis [7].

When a substrate that can transmit laser light is set on the laser-absorbing liquid, a high-energy state can be formed at the solid–liquid interface by irradiating the liquid through the transparent substrates (Fig. 10.2). More precisely, a high-energy state is formed in the thin liquid layer in contact with the transparent materials. When the liquid presents a higher absorbance at the laser wavelength, the liquid layer where the laser light is absorbed becomes thinner, resulting in a higher energy density. This high-energy state can act on the backside surface of the substrate and etch the surface gently. Wang et al. developed a surface micromachining technique employing this phenomenon and named it "Laser-induced backside wet etching (LIBWE)" [8].

10.2 Laser-Induced Backside Wet Etching (LIBWE) in the Initial Study

LIBWE is a technique for the laser surface micromachining of transparent materials, such as glasses. Because transparent materials are generally hard and brittle, precise micromachining is challenging; for example, cracks are easily formed. The same issue exists for laser processing. Moreover, the transparency of the materials makes laser processing inherently difficult, which is based on the energy deposition upon the optical absorption of materials. One important characteristic of LIBWE is the crack-free micromachining of the transparent materials. The indirect action of a

laser enables precise micromachining without crack formation; the laser energy is not absorbed directly by the transparent materials to be etched, but instead by the laser-absorbing liquid in contact with the transparent materials. A diagram of the LIBWE apparatus is shown in the Fig. 10.3.

In a study by Wang et al. [8], fused silica was etched by a KrF excimer laser ($\lambda = 248$ nm, FWHM 30 ns, pulse repetition 2 Hz) by employing an acetone solution containing pyrene with a concentration of 0.4 mol/dm^3. The laser light was patterned by a metal stencil mask and projected at the liquid–solid interface. The laser energy passing through the fused silica plate was absorbed by the solution at the interface. The concentration of the solution was nearly saturated, demonstrating a high absorbance at the laser wavelength. The optical penetration depth was evaluated as 0.7 μm. Etching showed the threshold for applied fluence similarly to the laser ablation; etching was observed at a fluence higher than the threshold of 240 mJ/cm^2. Therefore, the LIBWE has often been described as the etching based on the laser ablation of liquid. The threshold of LIBWE is significantly lower than the fluence required for direct laser ablation (>14 J/cm^2) [9]. The surface of the irradiated area was etched pulse by pulse above the threshold, as shown in Fig. 10.4. The etch rate was ranged from 5 to 25 nm/pulse for the applied laser fluence ranging from 400 to 1300 mJ/cm^2. Additionally, the fabrication of crack-free and debris-free microstructures was demonstrated on patterned irradiation, as shown in Fig. 10.5.

Several research groups have developed the LIBWE technique. The important characteristics of this technique are as follows:

(1) Micrometer-scale structures can be fabricated on the surface of hard and brittle transparent materials without debris or crack formation.

(2) Etching can be performed at a significantly lower fluence compared to that required for the direct ablation of materials.

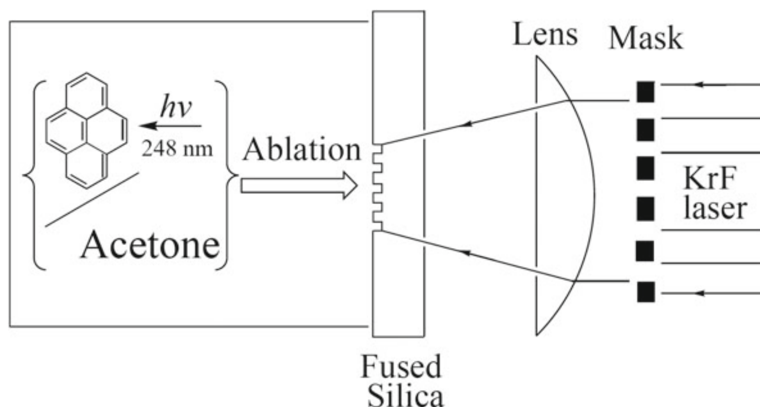

Fig. 10.3 Diagram of LIBWE apparatus used in Ref. [8]. Reprinted by permission from Springer: Ref [8], Copyright 1999.

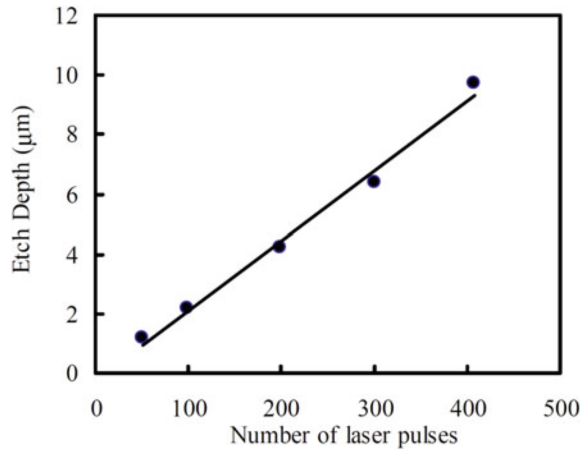

Fig. 10.4 Etch depths increased linearly with the number of applied laser pulses. Reprinted by permission from Springer: Ref [8], Copyright 1999.

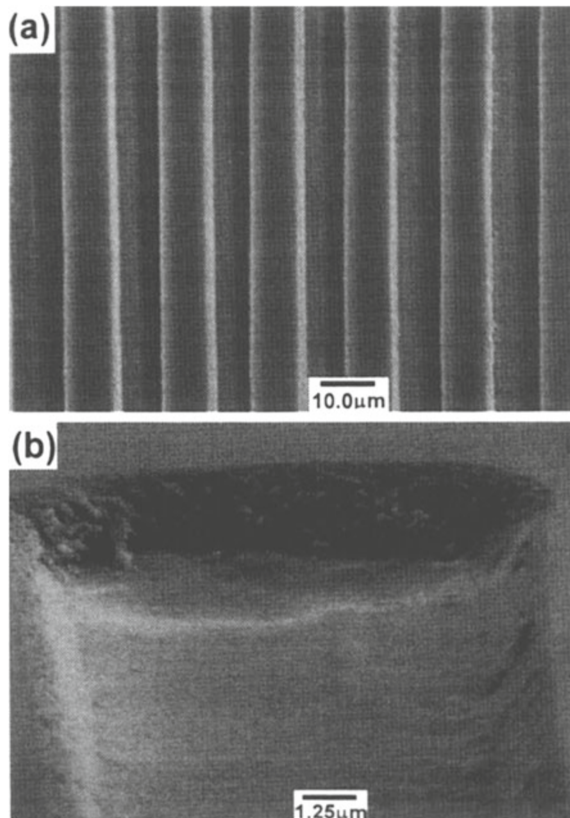

Fig. 10.5 Micrometer-scale lines and spaces pattern fabricated on the surface of fused silica. Reprinted by permission from Springer: Ref [8], Copyright 1999.

(3) The depth of etching increases linearly with the applied pulse numbers, enabling the fabrication of structures with high aspect ratios, whose depths can be precisely controlled.
(4) A smooth etched surface can be obtained.
(5) The apparatus used for general laser processing can be applied to this technique.
(6) Stable and reproducible processing can be executed upon accumulation of pulse irradiation.
(7) Various lasers and laser-absorbing liquids can be applied for the processing of various transparent materials.

Utilization of the indirect action of lasers is an effective method for the crack-free micromachining of hard and brittle transparent materials. Another indirect processing techniques utilizing the action of laser-induced plasma have been developed as the laser-induced plasma-assisted ablation (LIPAA) technique [10–14]. Additionally, laser etching at a surface-adsorbed layer (LESAL) [15] and laser-induced backside dry etching (LIBDE) [14, 16, 17] have been developed based on studies regarding LIBWE.

10.3 Variation in Combination of Lasers and Materials

The LIBWE process is based on the formation of the laser-induced high-energy state at the liquid–solid interface and its action on transparent materials. This simple concept of LIBWE has resulted in a wide variety of laser and material selection. However, a substantial limitation is that the laser energy sufficient for etching must reach the interface. Therefore, the optical transmittance at the laser wavelength is a key factor in the LIBWE process. Figure 10.6 presents the optical transmittance spectra of several transparent materials with indications of the wavelengths of typical lasers.

In a study by Wang et al. [8], a KrF excimer laser and fused silica plates were employed as the light source and the material to be etched, respectively. This combination came from the experiments on laser ablation of polymeric materials enhanced by dye molecules [18], where the transparent polymeric films containing dye molecules were ablated by UV pulses of a KrF excimer laser. Pyrene, a popular dye molecule used by photochemists, was chosen as the dye molecule for the experiments. Transparent polymeric films containing pyrene were prepared on fused silica substrates. When the polymer film was unintentionally irradiated through the substrate, the fused silica plate was unexpectedly damaged, despite the irradiated fluence being significantly below the damage threshold. To apply this phenomenon to the etching of fused silica, polymer films were replaced by an acetone solution containing pyrene. By employing the solution, the liquid–solid interface can be regenerated after each laser pulse irradiation, and deeper etching can be attained by repeated pulse irradiation. Acetone was selected as a solvent to dissolve pyrene at high concentrations. Note, similar damage formation had already been realized in an early study regarding the laser ablation of molecular liquids [2]. In this section, the

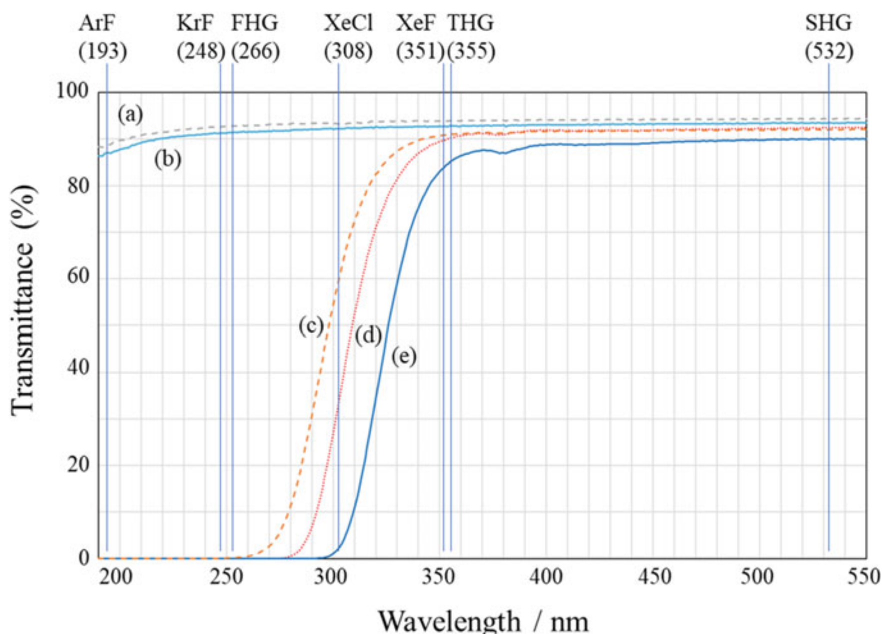

Fig. 10.6 Optical transmission spectra of representative transparent materials: **a** CaF_2 (2 mm), **b** fused silica (2 mm), **c** Corning gorilla glass, aluminosilicate glass (1 mm), **d** Corning Pyrex, borosilicate glass (2 mm), **e** soda-lime glass (1.75 mm); thickness indicated in parentheses

combinations of lasers and materials are discussed. Lasers, laser-absorbing liquids, and materials to be etched are listed with the types of experimental setups in Table 10.1. Note, the studies reporting the first usage of the combination are listed.

Precedent to the naming of LIBWE, there were several reports regarding the laser machining of transparent materials assisted by liquid media. Ikeno et al. had reported the etching of fused silica using a Nd:YAG laser ($\lambda = 1064$ nm, $\tau = 1$ ms, pulse energy 3 J/pulse) with a $NiSO_4$ aqueous solution (~2 mol/l) [19]. Hole drilling at the millimeter to sub-millimeter scale was performed by the focused irradiation of near-infrared (NIR) laser pulses. Dolgaev et al. reported the drilling of sapphire using a copper-vapor laser ($\lambda = 510$ nm, $\tau = 10$ ns, pulse repetition 8 kHz) [20, 21] combined with aqueous solutions of CrO_3, $KMnO_3$, and $FeCl_3$ or a highly dispersed suspension of carbon in toluene as a laser-absorbing liquid. These drilling processes originate from the high-energy states formed in the liquid layer. In these studies, it was concluded that the first action of the high-energy state is not the etching of the transparent materials, but the formation of absorbing oxide layers on the surface of the transparent materials [21]. The contributions of the deposited and/or modified layers for the LIBWE process are presented in a later section. Recently, similar processes were reported as LIBWE processes employing aqueous solutions of inorganic compounds combined with fundamental or second harmonic generation (SHG) pulses of diode-pumped solid-state (DPSS) lasers [22–28].

Table 10.1 Combinations of lasers, laser-absorbing liquids, materials to be etched, and types of the experimental setups in the LIBWE processes

Laser (wavelength)	Laser-absorbing liquid	Material to be etched	Type of experimental setup	References
ArF excimer (193)	Naphthalene/methylmethacrylate	Fused silica	Focused	[29]
KrF excimer (248)	Pyrene/acetone	Fused silica	Mask projection	[8]
	Pyrene/acetone	Quartz(c-SiO_2)	Mask projection	[30]
	Pyrene/acetone	CaF_2	Mask projection	[31]
	Pyrene/C_2Cl_4 Pyrene/cyclohexane	Fused silica Sapphire CaF_2 MgF_2	Mask projection Scanning counter mask	[32]
	Pyrene/toluene	Fused silica	Phase grating projection	[33]
	Pyrene/C_6H_5Cl Pyrene/$C_6H_4Cl_2$ Pyrene/C_6H_5F	Fused silica	Mask projection	[34]
	Toluene	Fused silica	Mask projection	[35]
	Toluene	Sapphire	Mask projection	[36]
	Phenolphthalein/N-methyl-2-pyrrolidone	Sapphire	Mask projection	[37]
	Naphthalene /methylmethacrylate	Fused silica	Focused	[38]
	Pyranine/water	Fused silica	Mask projection	[39]
	Naphthalene $(SO_3)_3Na_3$/water	Fused silica	Mask projection	[40]
	Liquid Ga	Fused silica	Mask projection	[41]
	Hg	Fused silica	Mask projection	[42]
	liquid Sn	Fused silica	Mask projection	[17]

(continued)

Table 10.1 (continued)

Laser (wavelength)	Laser-absorbing liquid	Material to be etched	Type of experimental setup	References
FHG of Solid Laser (266)	Pyrene/acetone Toluene *t*-butylbenzene Trimethylbenzene Naphthalene/Acetone Phenanthrene/acetone Anthracene/acetone 9-methylanthrathene/acetone 9,10-dimethylanthrathene/acetone Fluoranthene/acetone 9-phenylanthracene/acetone	Schott Borofloat33 (borosilicate glass)	Stage scan	[43]
	Toluene	Fused silica	Galvano scan	[44]
	C_6H_5Cl	Sapphire	Phase grating (interference)	[45]
	Naphthalene/methylmethacrylate	Fused silica	Beam interference	[46]
	Naphthalene/methylmethacrylate	SiO_2 film/fused silica Al_2O_3 film/fused silica Y_2O_3 film/fused silica	Beam interference	[47]
	Naphthalene/methylmethacrylate	HfO_2 film/fused silica ZrO_2 film/fused silica	Beam interference	[48]
XeCl excimer (308)	Pyrene/THF	FEP	Mask projection	[49]
	Pyrene/THF	Quartz	Mask projection	[50]
	Pyrene/acetone	Fused silica	Mask projection	[51]
	Pyrene/acetone	Quartz	Mask projection	[52]

(continued)

Table 10.1 (continued)

Laser (wavelength)	Laser-absorbing liquid	Material to be etched	Type of experimental setup	References
	Pyrene/acetone	CaF_2 BaF_2 Sapphire	Mask projection	[53]
XeF excimer (351)	Pyrene/acetone Pyrene/C_2Cl_4 Pyrene/cyclohexane	Corning pyrex, 7059 Schott D263, AF45 (borosilicate glass)	Mask projection	[54]
	Pyranine/water	Fused silica	Mask projection	[39]
THG of Solid Laser (355)	Pyrene/toluene Toluene	Quartz	Galvano scan	[55]
	Toluene	Fused silica	Galvano scan	[56]
	Toluene	Sapphire MgF_2 CaF_2	Galvano scan	[57]
Cu vapor (510)	CrO_3/water $KMnO_4$/water Carbon (suspended)/toluene	Sapphire	Stage scan	[20]
	$FeCl_3$/water	Sapphire	Stage scan	[21]
SHG of Solid Laser (515)	$KMnO_4$ / water	SiO_2	Galvano scan	[22]
SHG of Solid Laser (527)	$AgNO_3$/water Amaranth/water	Silicate glass	Stage scan	[23]
	Amaranth + PEG/water	Silicate glass	Focused	[58]
	$AgNO_3$ / water	Sapphire	Stage scan	[24]

(continued)

Table 10.1 (continued)

Laser (wavelength)	Laser-absorbing liquid	Material to be etched	Type of experimental setup	References
SHG of Solid Laser (532)	Rose bengal/acetone	Soda-lime glass	Stage scan	[59]
	Rose bengal/water	ITO-coated glass	Stage scan	[60]
	Rhodamine 6G/ethanol–toluene	Fused silica	Galvano scan	[61]
	Oil-Red-O/*p*-xylene	Borosilicate glass	Stage scan	[62]
	Sudan IV/toluene	Soda-lime glass	Galvano scan with beam interference	[63]
	$KMnO_4$ / water	PMMA	Stage scan	[25]
	Liquid Ga In–Ga	Soda-lime glass Quartz	Stage scan	[64]
	Liquid Ga	Fused silica fiber	Dipping	[65]
	In–Ga	Zerodur	Stage scan	[66]
	In–Ga	PMMA	Stage scan	[67]
Fundamental of Solid Laser (1064)	$NiSO_4$ / water	Fused silica	Focused	[19]
	$CuSO_4$ /water	Soda-lime glass	Galvano scan	[26]
	$CuSO_4$ /water	Sapphire	Galvano scan	[27]
	$CuSO_4$ + phosphoric acid /water	Soda-lime glass	Galvano scan	[28]
	Liquid Ga	Fused silica	Focused	[68]
	In–Ga	NaCl	Focused	[69]

After the naming of LIBWE, etching employing excimer lasers (ArF (λ = 193 nm), KrF (λ = 248 nm), XeCl (λ = 308 nm), and XeF (λ = 351 nm)) has been reported by several research groups. The number of studies employing a KrF excimer laser is larger than that using other excimer lasers, which may be due to the fact that the optical absorption ascribed to the π-π* transition of the benzene ring is located at approximately 250 nm, and a wide variety of molecules containing benzene rings can be used as absorbers. The materials to be etched were fused silica, quartz (SiO_2 crystal), sapphire, and fluoride crystals (CaF_2, MgF_2, and BaF_2). These materials can transmit laser pulses at UV wavelengths. Wang et al. reported the etching of a UV-transparent fluoropolymer (FEP) film [49]. One exceptional case is the study by Cheng et al., who reported the etching of Borofloat33 (Schott), which is a type of borosilicate glass, with the fourth harmonic generation (FHG) pulses (λ = 266 nm) of a DPSS laser [43]. As shown in Fig. 10.6, pyrex classified to borosilicate glasses presents an absorption edge at approximately 350 nm, and no transmittance at 266 nm. It was reported that a Borofloat33 glass with a thickness of 0.7 mm absorbed 50% of the laser energy. Thus, the remaining 50% reached the interface and was used for the crack-free fabrication of microtrenches. This study revealed that the LIBWE of the materials that weakly absorbs the laser energy is executable if sufficient energy reaches the interface without causing damage to the substrates. When a XeF excimer laser that emits laser pulses with the wavelength of 351 nm is used for LIBWE, the etching of borosilicate glasses (Corning, Pyrex, 7059, Schott D263, AF45) can be performed as a processing of highly transparent materials [54].

Pyrene is a major dye molecule used in LIBWE. Several organic solvents such as acetone, tetrahydrofuran, toluene, cyclohexane, and tetrachloroethylene (C_2Cl_4) are used to dissolve it. Because molecules with benzene rings present an optical absorption near 250 nm, toluene and other substituted benzenes can be used as laser-absorbing dye molecules [35, 36, 43–45]. Cheng et al. investigated the threshold fluences of LIBWE for 11 organic laser-absorbing liquids and confirmed that the unit length absorbance, which is related to the optical penetration lengths, correlated with the obtained threshold values [43]. Vass et al. used a solution of naphthalene dissolved in methylmethacrylate for LIBWE with ArF [29] and KrF [38] excimer lasers as well as FHG pulses of the Nd:YAG laser [46–48]. Fujito et al. employed a solution of phenolphthalein dissolved in N-methyl-2-pyrrolidone for the etching of sapphire [37]. Aqueous dye solutions have adapted for LIBWE by Ding et al.; pyranine [39] and naphthalene-1,3,5-trisulfonic acid trisodium salt ($Np(SO_3)_3Na_3$) [40] were employed as dye molecules. Thus, a wide variety of dye molecules can be used in the LIBWE employing the UV lasers.

The green emission of SHG pulses of solid lasers in visible range (λ = 515, 527, and 532 nm) can be used for LIBWE. As shown in Fig. 10.6, all transparent materials present a sufficient transmittance at this wavelength. Cheng et al. developed the LIBWE employing SHG pulses and named it visible LIBWE [59]. Soda-lime glasses, the most commonly available glass used for windows in buildings, whose absorption edges are located near 380 nm, can be etched by employing the visible wavelengths. Tsvetkov et al. employed an aqueous solution containing Amaranth, a red food dye [23, 58]. Moreover, polyethylene glycol (PEG) was added to the solution

to reduce the surface tension of the liquid, which affected the cavitation behavior, which will be described later.

Liquid metal was also used for etching. Etching using liquid-phase gallium combined with a KrF excimer laser was first reported by Zimmer et al., which presents one-order higher etch rates than the LIBWE employing an organic dye solution [41]. The low melting point of gallium (29.76 ºC) enables its use in the liquid phase upon heating. Although high reflectivity causes energy loss, the penetration depth of light is relatively small. Therefore, metals in the liquid phase can be good laser-absorbing liquids for the LIBWE process, which can be used for a wide range of wavelengths. Zimmer et al. reported the etching of fused silica by fundamental laser pulses of the Nd:YAG laser ($\lambda = 1064$ nm) [68]. Studies employing mercury [42] and molten tin [17] have been reported. Eutectic indium/gallium alloy (In–Ga) can be used for visible LIBWE without heating [64, 66, 67, 69].

10.4 Variation in Experimental Setups for LIBWE

In addition to the combination of lasers and materials, the simple concept of LIBWE also results in variation of the setups for irradiation. In this section, the experimental setups for LIBWE are reviewed.

10.4.1 Mask Projection with Excimer Laser

Because excimer lasers can emit laser pulses with large areas, they can be used for patterned irradiation by mask projection. This technique is similar to that used in the photolithography processes for semiconductor device production. Therefore, setups for patterned irradiation with homogeneous light intensity have been established and enable precise surface micromachining. It was reported that smooth surface with low roughness of 50 nm could be obtained by employing this type of apparatus [52, 70]. The fabrication of micro-optical devices has been demonstrated [32, 52, 70, 71].

Initially, we used simple experimental setups equipped by ourselves with a metal stencil mask and a planoconvex lens for each experiment. Although the fabrication of microstructures can be demonstrated, the quality of fabrication is occasionally not exceptional [51]. Beam shaping and the precise positioning of samples to match the liquid–solid interface with the imaging plane of the optical system enable high-quality machining, as shown in Fig. 10.7; for fabricating the structure, Böhme et al. used an irradiation setup with projection optics having a resolution of 5.0 and 1.5 μm [32].

We introduced a machining setup composed of beam homogenizer, dielectric attenuator, chromium-on-quartz-masks, as well as an $\times$ 8 demagnification objective (MicroLas Lasersystem GmbH), and a motorized x–y–z stage for the sample positioning (Fig. 10.8). The resolution limit of this system was specified as 3 μm lines

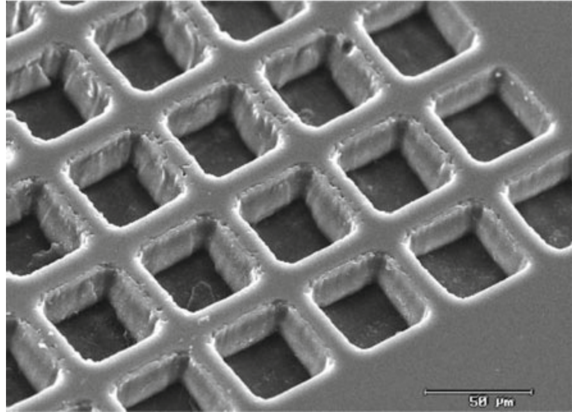

Fig. 10.7 Surface structure of fused silica fabricated by Böhme et al. Reprinted from Ref. [32], Copyright (2002), with permission from Elsevier.

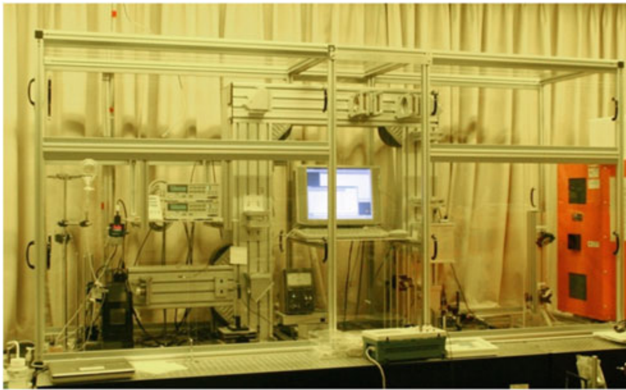

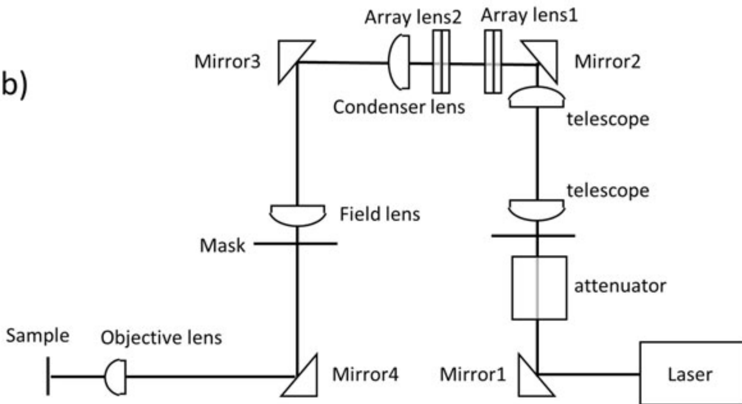

Fig. 10.8 **a** An image and **b** layout of the new setup for the mask projection LIBWE

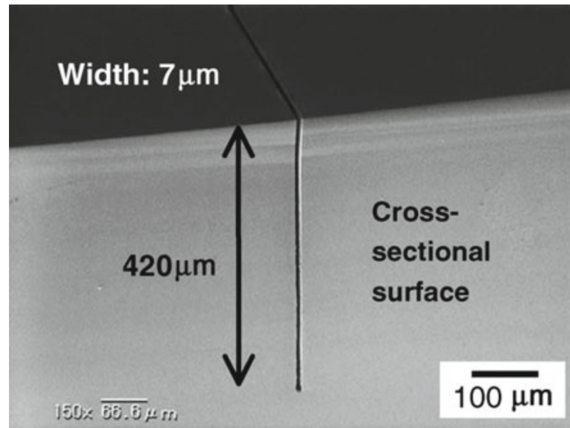

Fig. 10.9 Cross-sectional SEM image of deep microtrench fabricated with adjusting dynamically the sample position for matching the etch front to the imaging plane of the optical system. Reprinted from Ref. [74], Copyright (2006), with permission from Elsevier.

and spaces. The quality and reproducibility of microfabrication improved by using this system [36]. A precise control of the sample position within ± 15 µm to match the liquid–solid interface with the imaging plane of the optical system is required for precise etching [72]. We developed a system to compensate for the inclination of the surface and the displacement induced by the surrounding temperature change; the fabrication of microstructures with homogeneous quality over a wide area on the fused silica plates was then attained. Based on the precise positioning of samples, the fabrication of deep microtrenches and holes with high aspect ratios was performed (Fig. 10.9) [72–77]. This type of fabrication can be achieved by locating dynamically the etch front, which in this case was the bottom of the trenches, at the imaging plane of the optical system.

10.4.2 Etching on Interference

The spatial resolution of the mask projection systems is limited by optical systems. To achieve a higher resolution, the interference of laser beams was applied for etching. Zimmer et al. reported the fabrication of a surface relief grating with a period of 780 nm by phase grating projection using a Schwarzschild objective [33]. The sub-micron resolution of LIBWE was proven in this study. Vass et al. demonstrated the fabrication of surface relief grating with a shorter period by a two-beam interference of FHG pulses of the Nd:YAG laser with incident angles up to 60° [46]. They named this method TWIN-LIBWE and fabricated surface relief gratings with various periods, the smallest period was 104 nm (Fig. 10.10) [47, 48, 78–81].

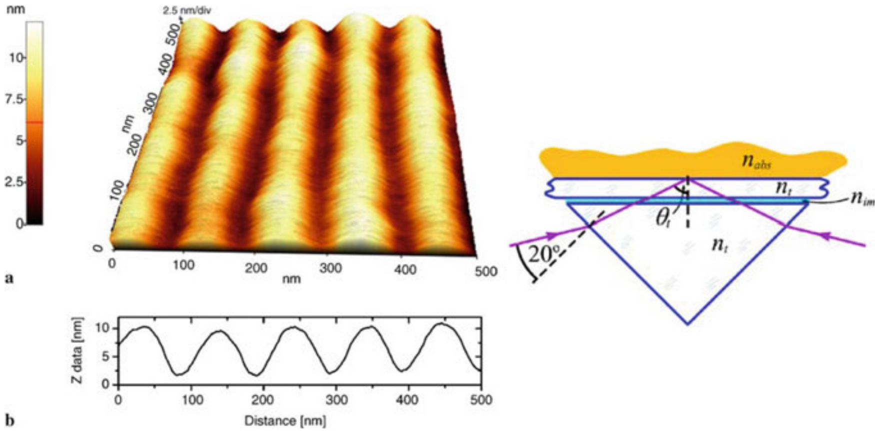

Fig. 10.10 Surface relief grating with period of 104 nm fabricated by the immersion TWIN-LIBWE. Reprinted by permission from Springer: Ref [78], Copyright 2007.

10.4.3 Direct-Writing by Scanning with High Repetition

Laser-Direct-Write (LDW) is an attractive technique that enables versatile material processing with patterns in scales ranging from nanometers to millimeters [82], where lasers with a high pulse repetition (~100 kHz) are employed for computer-controlled two- and three-dimensional pattern formation in a serial fashion. LDW with LIBWE was first demonstrated by Cheng et al. using computer numerical control (CNC) stages and a DPSS laser operated with a pulse repetition of 4.5 kHz [43]. Microchannel structures for microfluidic chips were fabricated on borosilicate glass. A direct write with beam scanning by a galvanometer-based point scanning system was demonstrated by Niino et al. [44, 83] (Fig. 10.11), where a DPSS laser was operated at a 10 kHz pulse repetition and used for flexible mask-less processing. This type of LIBWE can be used for the laser marking of glass materials (Fig. 10.12) [44, 63, 84].

10.5 Various Studies Regarding the Elucidation of the LIBWE Mechanisms

While the basic concept of the LIBWE is simple, the mechanisms involved are complex. The mechanism of material removal has not yet been fully understood. Several processes would be involved in the etching phenomena, and their contributions may be altered by the applied materials and conditions of laser irradiation. The wide variety of materials and conditions for LIBWE makes the situation more

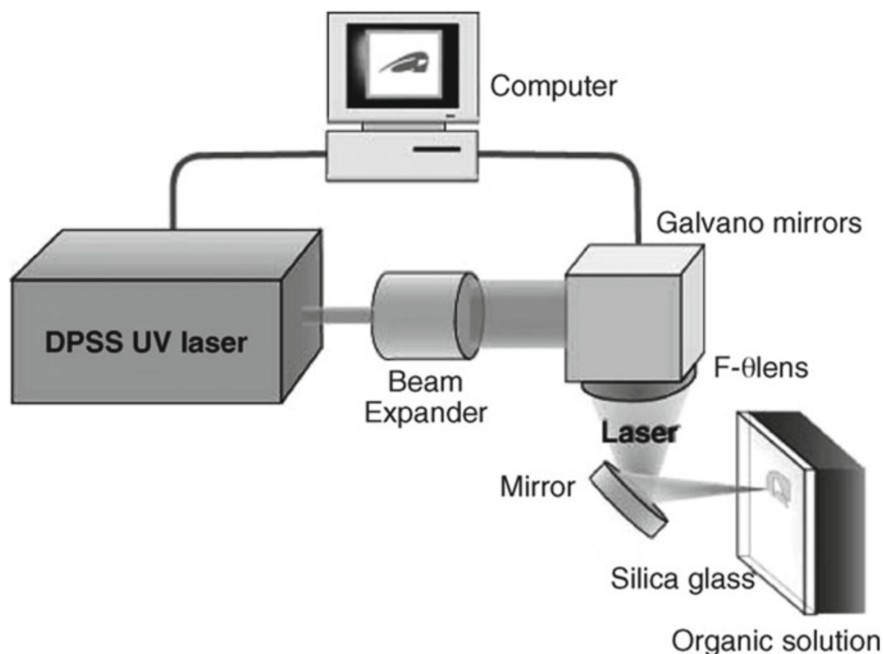

Fig. 11 Setup for LDW LIBWE employing the galvanometer-based point scanning system with a DPSS laser. Reprinted from Ref. [83], Copyright (2007), with permission from Elsevier.

complex. Discussions and diagnostic studies addressing the elemental phenomena are overviewed.

10.5.1 Estimation of Temperature Rise

In the initial studies, the temperature increase in the thin liquid layers was evaluated using the absorbed laser energy, liquid volume that absorbed laser light obtained from the optical penetration depth, and the heat capacity of the solvent [8, 52]. The maximum temperatures of the liquid layer were evaluated as 1900–2300 K, which is above the softening and melting temperatures of fused silica. Wang et al. discussed on the involvement of super-heated liquid [31] produced by heating within a pulse duration based on a cyclic multiphotonic absorption mechanism [85]. Note, the transient imaging of the interface indicated that the initial flat bubbles before expansion were observed at a delay time of 100 ns [35, 40, 86]. Organic molecules are decomposed at such high temperature. Partial decomposition of organic molecules was indicated by emission of gas bubbles with the distinctive odor of sulfur-containing gas [39], or by production of carbon soot from photolyzed toluene [35]. Note, the emitted gas bubbles should be distinguished from the cavitation bubbles that will be

described later. Kopitkovas et al. reported that the difference in the threshold fluences obtained for the LIBWE by KrF and XeCl lasers can be explained by the calculated induced temperatures reaching the melting point of quartz (1880 K) as shown in Fig. 10.13 [52]. However, as indicated by Vass et al., the temperature of the solid target was not calculated in these studies. They evaluated the temperature of a solid target by numerical calculations using the method of finite differences [29, 86]. The surface of the solid target was concluded to reach the melting point; the depths of the melting layers formed upon irradiation at various fluences were also evaluated (Fig. 10.14). The difference between etch depth and calculated maximum depth of the melted layer was ascribed to the partial removal of the melted fused silica. On

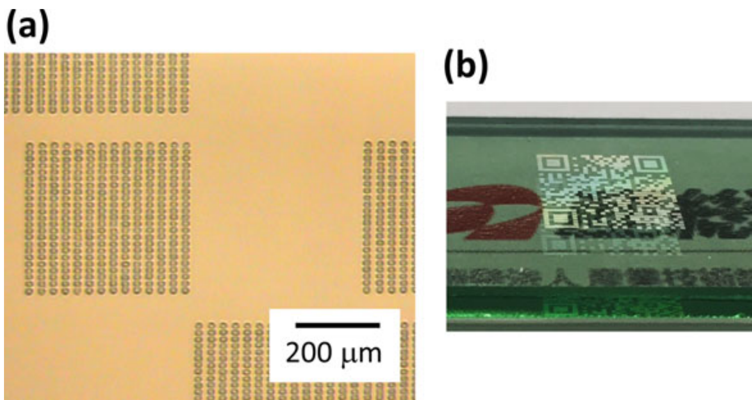

Fig. 10.12 Laser marking on glass by LIBWE with **a** micropit array structures for writing **b** a QR code on a soda-lime glass plate. Reproduced from Ref. [84] with permission from Japan Laser Processing Society.

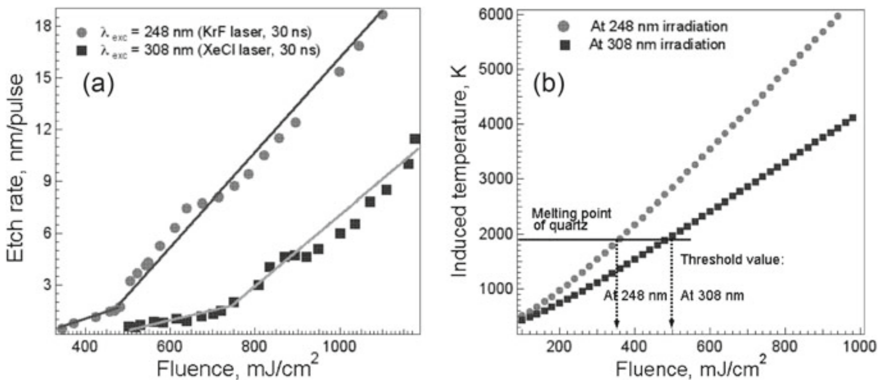

Fig. 10.13 **a** Etch rates dependent on the laser fluence presenting two-stage behaviors in the LIBWE employing the KrF and XeCl laser. **b** Calculated temperature at the quartz-liquid interface as a function of the laser fluence. Reprinted from Ref. [52], Copyright (2003), with permission from Elsevier.

the other hand, an analytical solution of the laser-induced temperature distribution was evaluated by Zimmer [87]. He argued that the temperature of the surface of the solid target did not reach the melting point without the existence of the interface absorption. The existence of a modified layer with interface absorption was proven, which will be described later.

10.5.2 Etch Rates and Threshold Values

The threshold fluence and the etch rate have been focused in the studies on LIBWE as the parameters characterizing the processes. Böhme et al. first realized that the etch rates dependent on the fluence were fitted by two lines in different fluence ranges [32]. As shown in Fig. 10.13, similar two-stage behaviors were confirmed in different studies [40, 52, 53, 70, 86]. This appears to be a general behavior for LIBWE, indicating that different mechanisms are involved in the etching process. Note, the etch rate of LIBWE can be varied with spot size for irradiation, as shown in Fig. 10.15 [88]. The experimental results obtained under different conditions should be treated with care.

The incubation effect in the LIBWE is shown in Fig. 10.15. The existence of this effect was first reported by Yasui et al. [51] in the etching of fused silica with a XeCl excimer laser at the fluence of 0.4 J/cm^2; etching was not discerned upon irradiation with 3000 pulses, while etching with the depth of 0.4 μm was observed upon irradiation with 5000 pulses. Similar behavior was observed for the etching of quartz by a XeCl excimer laser at low fluences (1.18 J/cm^2), just above the threshold; start of the etching was observed upon irradiation with more than 150 laser pulses [53]. The existence of the incubation effect revealed the involvement of an initial process causing the generation of absorbing sites, such as defects. Ding et al. confirmed that

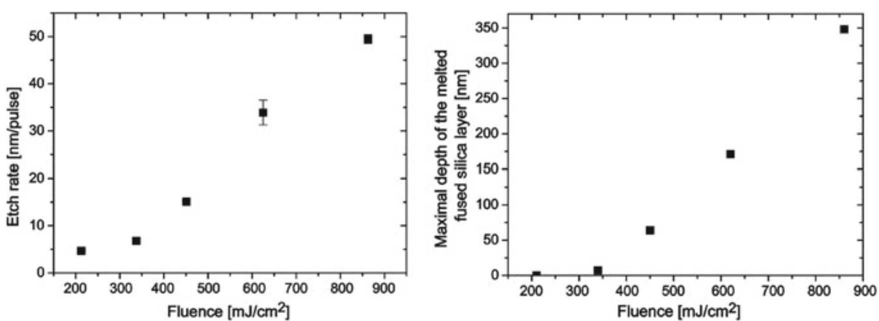

Fig. 10.14 (left) Etch rates versus laser fluence for LIBWE employing an ArF excimer laser and naphthalene/methylmethacrylate, (right) the maximum depth of the melted fused silica layer calculated by the method of finite differences. Reprinted from Ref. [29], Copyright (2004), with permission from Elsevier.

the etching of sapphire started after the etched area was covered with black particles of amorphous carbon [36]. On the other hand, the etching from a single laser pulse was confirmed at a sufficiently high fluence [53]. Single-shot etching was also confirmed in LIBWE employing focused laser pulses of DPSS lasers [84, 89].

10.5.3 Characterization of Etched Surface.

Etched surfaces were evaluated using Rutherford backscattering spectroscopy (RBS) [90], X-ray photoelectron spectroscopy (XPS) [90–92], Raman scattering spectroscopy [90, 91], fiber-tip ATR-IR spectroscopy [91], and ellipsometry [92]. The Raman spectra of the etched surface indicated the presence of amorphous carbon deposits, while chemical modification of fused silica was indicated by the XPS and fiber-tip ATR-IR results. Thus, not only the adhered amorphous carbon deposit layer, but also the formation of a modified layer in LIBWE was indicated. RBS measurements indicated the generation of an amorphization layer on quartz crystals with a thickness of up to 60 nm. The formation of a modified layer on fused silica with a thickness of 10–30 nm with an absorption coefficient of 100,000–180,000 cm^{-1} was indicated by ellipsometry. Zimmer et al. evaluated the absorption coefficient of the modified layer by local absorption measurements for a surface prepared by the ion beam beveling technique (Fig. 10.16) [93]. The existence of a modified layer on fused silica with a thickness less than 25 nm with a high absorption coefficient of 40×10^4 cm^{-1} was indicated. The thickness of a few tens nm was indicated in several observations and coincident with the typical etch rates obtained for LIBWE with excimer lasers. Based on the confirmation of the existence of a modified layer, they proposed a new mechanism of LIBWE composed of the formation of a modified layer and its direct ablation [94].

10.5.4 Diagnostic Studies on LIBWE

To address the mechanism of LIBWE, diagnostic studies using several in situ measurements have been applied. As previously indicated, a rapid temperature increase in the liquid layer causes cavitation in the liquid. The cavitation behaviors were observed by transient imaging using the shadow graph technique, as shown in Fig. 10.17 [35, 40, 86, 95–97], and in situ reflectivity measurements [61, 98]. Based on the dynamics of a bubble, the pressure inside of a bubble can be evaluated based on the following physical model [99]:

$$p\left(R, \frac{dR}{dt}\right) = \left(p_{stat} + \frac{2\sigma}{R_n}\right)\left(\frac{R_n}{R}\right)^{3\kappa} - \frac{2\sigma}{R} - \frac{4\mu}{R}\frac{dR}{dt} \qquad (10.1)$$

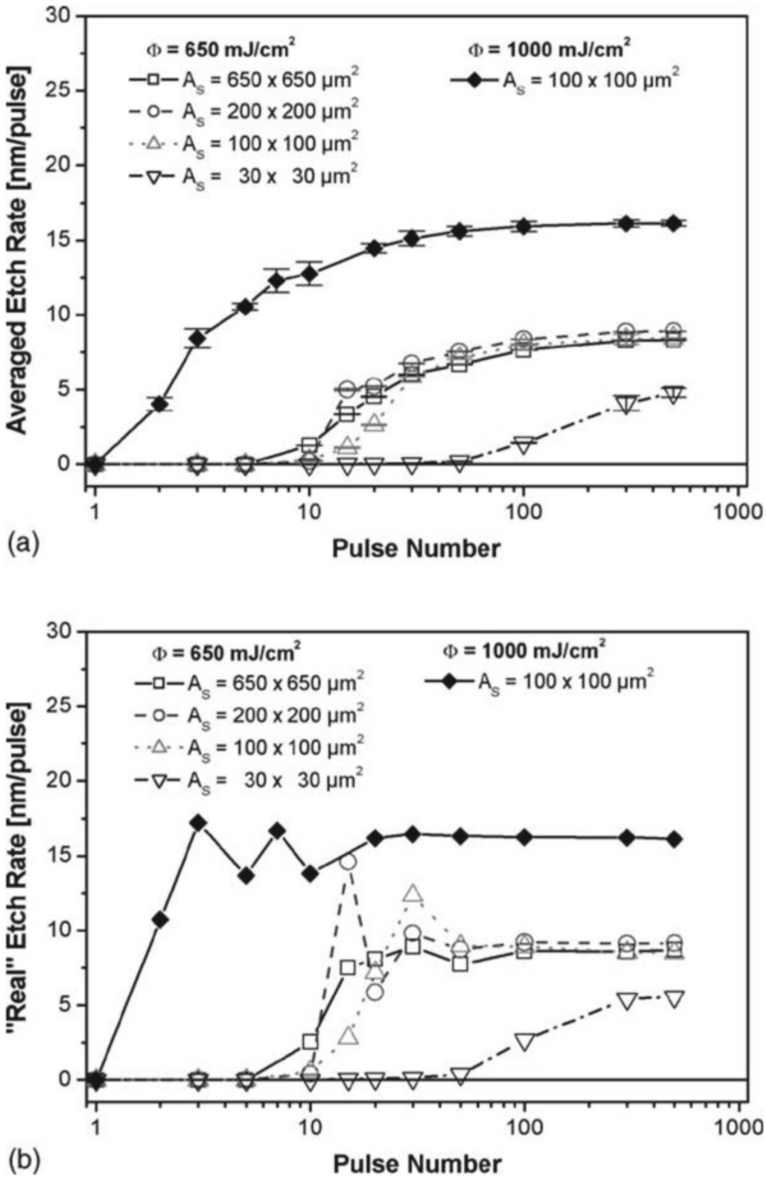

Fig. 10.15 **a** Averaged etch rate in dependent on the applied pulse number for difference spot sizes. **b** Calculated "real" etch rate per laser pulse. Reprinted from Ref. [88], Copyright (2005), with permission from Elsevier.

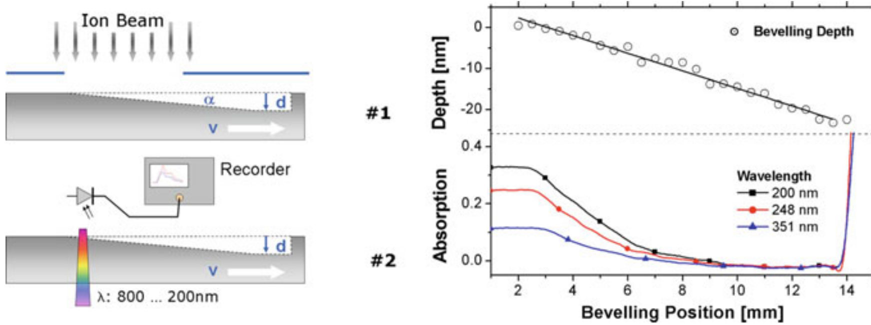

Fig. 10.16 (left) Schematic illustration of the preparation of the sample by ion beam beveling (#1) and the near-surface local absorption measurement (#2). (right) Measured etch depth and absorption at different positions of beveling. Reprinted from Ref. [93] with permission from AIP Publishing.

where R is the radius, R_n is the equilibrium radius of the bubble, p_{stat} is the statistic ambient air pressure, σ is the surface tension, μ is the dynamic shear viscosity, and κ is the polytropic exponent of the solvent. Vass et al. calculated an initial high pressure of approximately 70 MPa, which decreased instantly with the expansion of the bubble [86]. This initial high pressure was considered to remove the melted material from the surface. The generated initial high pressure propagates in the liquid as a shockwave, which can be detected using a piezoelectric pressure gauge [44, 58, 84, 89, 96, 97]. The initial pressure of 65 MPa deduced from the distance dependence was in the same order with the pressure obtained from the cavitation dynamics [97]. Meanwhile, cavitation dynamics indicate that the high-pressure is generated once again when cavitation bubble collapsed. Pairs of pressure signals corresponding to the formation and collapse of the cavitation bubble were observed (Fig. 10.18) [44, 84, 89]. The single-shot etching behavior was confirmed to be correlated to the cavitation behavior [84]. A micropit with a diameter of approximately 30 μm and the maximum depth up to 0.35 μm was fabricated by single-pulse irradiation. The maximum depths of micropits fabricated by two laser pulses with different time intervals are shown in Fig. 10.19; the etching with depth of approximately 0.6 μm was confirmed at the time interval larger than 125 μs, while etch depths became the half of them at the time interval less than 60 μs. Because the lifetime of cavitation bubble was evaluated as 63.2 ± 0.9 μs for the applied pulse energy of 44.0 μJ/pulse, these results revealed that the etching by the second pulse irradiated before collapsing of the cavitation bubble was completely suppressed. Moreover, decreased etch depths at the time intervals between 70 and 120 μs indicated partial suppression due to the formation of the second bubble [95]. The suppression of the etching by the second pulse in the successive two pulses was clearly observed in the etching with beam scanning. Figure 10.20 shows the micropit array fabricated with pulse repetition and scan speed of (a) 10 kHz and 750 mm/s and (b) 20 kHz and 1500 mm/s, respectively; laser pulses were delivered at every 75 μm in both cases. When the pulse repetition was 20 kHz, time interval of laser pulses of 50 μs was shorter than the lifetime

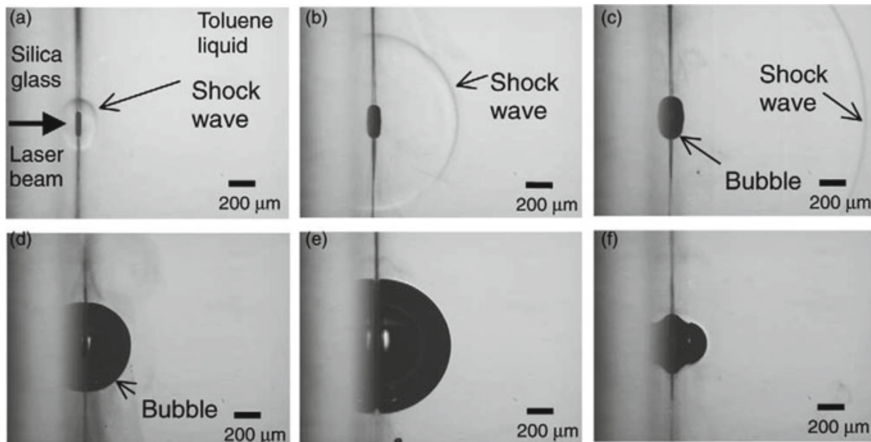

Fig. 10.17 Time-resolved optical images of the cavitation bubble formed by a KrF excimer laser irradiation on the interface between toluene and fused silica at the delay time of **a** 100 ns, **b** 500 ns, **c** 1.2 μs, **d** 10 μs, **e** 50 μs, and **f** 100 μs. Reprinted from Ref. [35], Copyright (2003), with permission from Elsevier.

of the cavitation bubble. As shown in Fig. 10.17, the bubble expands to out of the irradiated area. Thus, the suppression of the etching by every second pulse was induced (Fig. 10.20). Given the results that the self-assembled monolayer (SAM) on the fused silica around the irradiated area kept their function as reported by Ding et al. [100, 101], gas phase chemicals inside the bubble induced minor effect on the surface around the irradiated areas.

Although the results on single-shot LIBWE indicated the required action of liquid for etching, the involvement of the surface modification was not ruled out. The modified layer generation within the pulse duration was detected by time-resolved reflection measurements, as shown in Fig. 10.21 [94]. An increase in reflectivity observed within 15 ns indicated the generation of the modified layer within the pulse duration. Meanwhile, the etch depth of up to 0.35 μm in the single-shot LIBWE [84] would be larger than the thickness of the modified layer, that are coincident with the typical etch rates of a few tens nanometer. There should be additional mechanisms for material removal. In a similar single-shot LIBWE, the decrease in etch rates by adding PEG to the laser-absorbing liquid was confirmed [58]. The addition of PEG as a surfactant reduces the surface tension of the liquid and results in a decrease in the cavitation pressure as indicated by the measured pressure signal. The results indicate that the removal of melted material by the initial high pressure of cavitation is a possible additional mechanism. In the same study, the authors discussed the role of etching with supercritical water. However, given the etching is relatively slow, an etch rate of ca. 1 μm/min was observed in the etching of glass with supercritical water [102], the role of etching with supercritical water would be minor.

The blue light plasma emission, including the atomic lines of Ca and Al, was detected by Cheng et al., which indicated the direct ablation of glass materials [103].

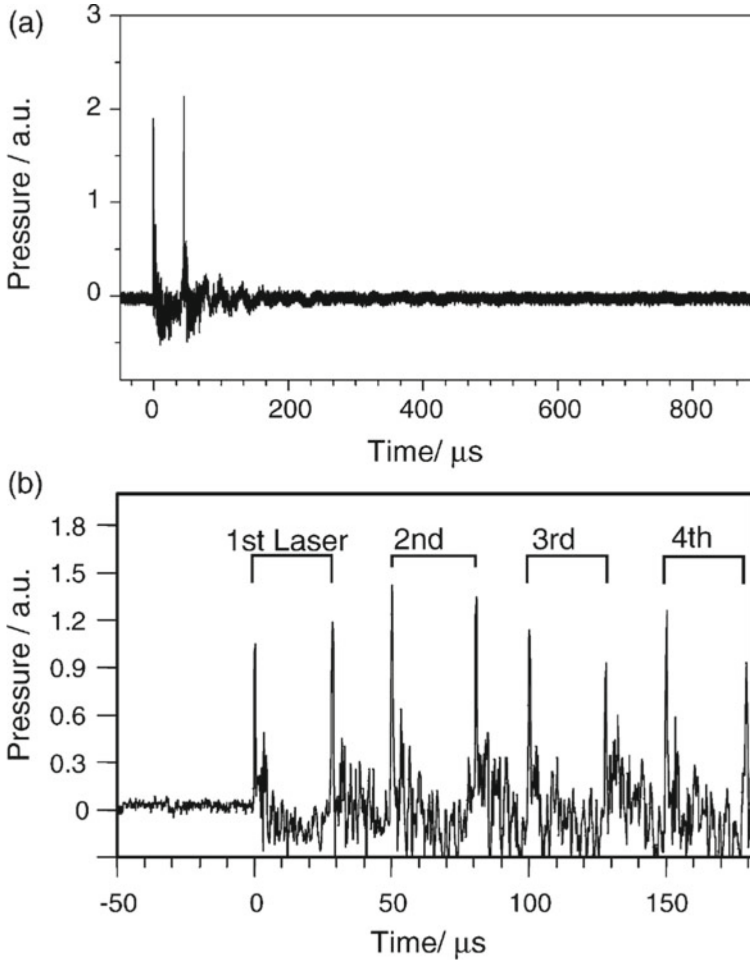

Fig. 10.18 Transient pressure signals observed in LIBWE using toluene and DPSS UV lasers at **a** 1 kHz (fluence: 520 mJ cm^{-2}, laser spot: 50 µm) and **b** 20 kHz (fluence: 5.7 J cm^{-2}, laser spot: 12 µm). Reprinted from Ref. [44], Copyright (2006), with permission from Elsevier.

Meanwhile, in the visible LIBWE of PMMA with In–Ga, the plasma emission of In and Ga was observed [67], which indicated plasma formation from the liquid media. The etching of transparent materials assisted by laser-induced plasma has been studied as LIPAA. In these studies, it was confirmed that the major role of plasma in LIPAA was the creation of an absorption site at the surface of the material [13, 14]. In the LIBWE process, the laser-induced plasma may contribute to the generation of an absorption site.

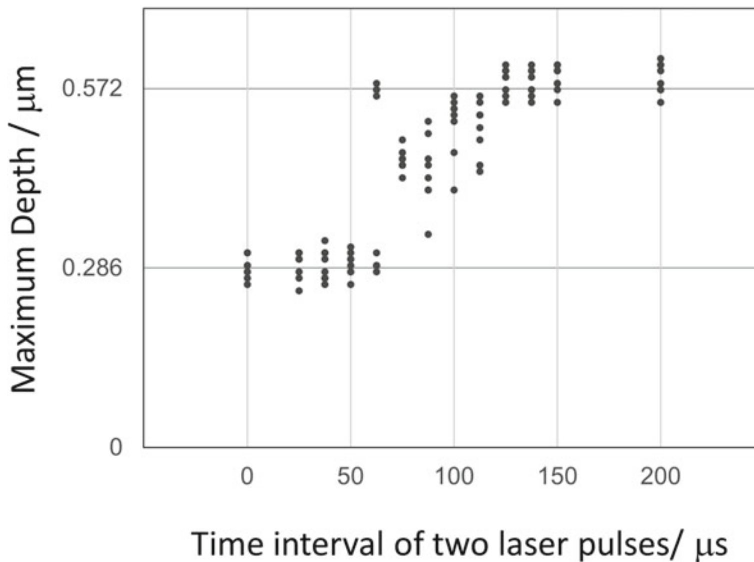

Fig. 10.19 Maximum depths of the micropits fabricated with two laser pulses with different time intervals. Reproduced from Ref. [84] with permission from Japan Laser Processing Society.

10.6 Summary

In this chapter, studies regarding the LIBWE process, that is the laser processing based on the action of high-energy states formed in liquid layer, are reviewed. This process achieves crack-free and debris-free precise micromachining of transparent materials. Therefore, it can be applied to fabricate micro-optical and microfluidic devices. The simple concept of this technique for utilizing the high-energy state in liquid allows a variety of combinations of lasers and materials as well as a variety of experimental setups for processing. While the concept for processing is simple, the mechanism of material removal, the action of the generated high-energy states, is rather complex. Several studies have been conducted to elucidate the actions of the high-energy states for material removal, which revealed that several mechanisms with different contribution ratios are involved in this process. One important mechanism is that the surface layer of the materials is modified by the chemical species formed in the high-energy state, and direct laser ablation of the laser-absorbing modified layer is induced. This phenomenon can be induced within a single-pulse duration. This process would be a major mechanism in the fabrication of microstructures on silica-based transparent materials with organic laser-absorbing liquid that shows a low etch rate up to a few tens of nanometers per pulse. For the etching of sapphire, the adhered amorphous carbon layer would be act as the interface absorbing layer. However, it is not clear that similar mechanism is involved in the etching of fluoride crystals or polymeric materials, or the etching employing liquid metallic absorbers. In addition

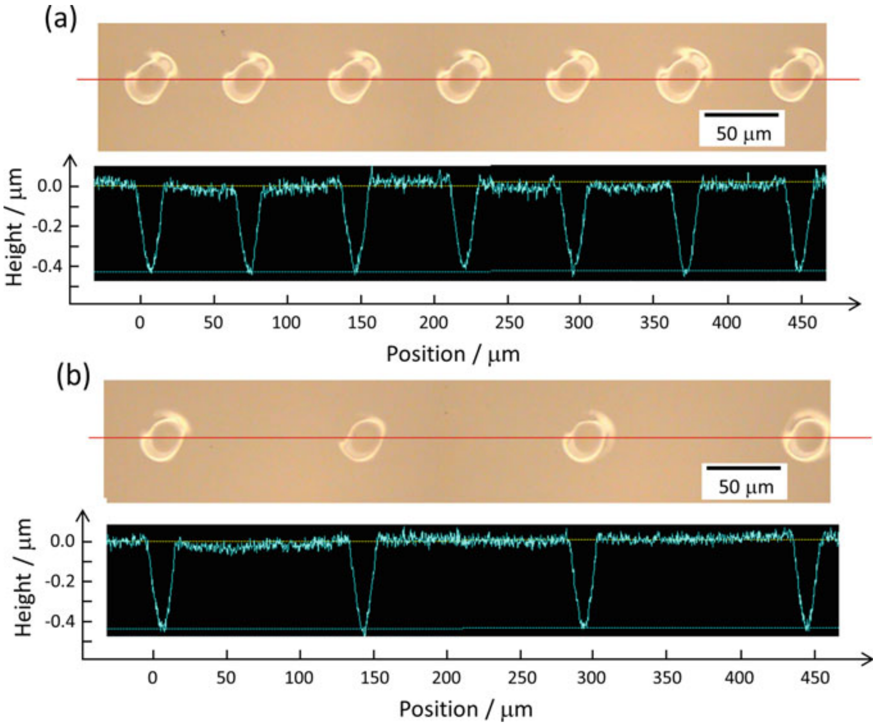

Fig. 10.20 Micropit array structures fabricated with pulse repetition and scan speed of **a** 10 kHz and 750 mm/s, **b** 20 kHz and 1500 mm/s, respectively. Reproduced from Ref. [84] with permission from Japan Laser Processing Society.

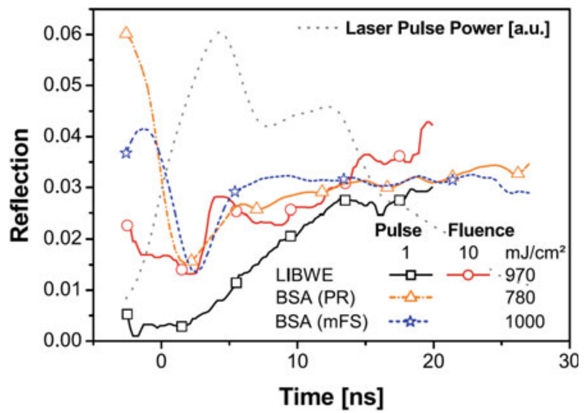

Fig. 10.21 Time-resolved reflection measurements at 248 nm for LIBWE and the backside ablation (BSA) of a 100-nm thick photoresist film on fused silica (PR) and LIBWE-modified fused silica (mFS). Reprinted by permission from Springer: Ref [94], Copyright 2010.

to the direct ablation of the modified layer, the mechanical removal of melted material by the high pressure induced in the initial stage of cavitation would be involved in the etching process induced at a higher fluence. An increased contribution of the latter mechanism was observed in the LDW-type LIBWE demonstrating incubation-free etching.

References

1. W. M. Steen, J. Mazumder, Laser Materials Processing, 4th ed., Springer-Verlog London, 2010
2. R. Srinivasan, A.P. Ghosh, Ablation of liquid benzene by pulsed ultraviolet (248 or 308 nm) laser radiation. Chem. Phys. Lett. **143**, 546–550 (1988). https://doi.org/10.1016/0009-2614(88)87064-7
3. S. Georgiou, A. Koubenakis, Laser-induced material ejection from model molecular solids and liquids: mechanisms, implications, and applications. Chem. Rev. **103**, 349–394 (2003). https://doi.org/10.1021/cr010429o
4. Y. Tsuboi, H. Fukumura, H. Masuhara, Nanosecond imaging study on laser ablation of liquid benzene. Appl. Phys. Lett. **64**, 2745–2747 (1994). https://doi.org/10.1063/1.111461
5. Y. Tsuboi, K. Hatanaka, H. Fukumura, H. Masuhara, The 248 nm excimer laser ablation of liquid benzene derivatives: a relation between ablation threshold and molecular photochemical reactivity. J. Phys. Chem. **98**, 11237–11241 (1994). https://doi.org/10.1021/j100095a001
6. K. Hatanaka, M. Kawao, Y. Tsuboi, H. Fukumura, H. Masuhara, Switching from photochemical to photothermal mechanism in laser ablation of benzene solutions. J. Appl. Phys. **82**, 5799–5806 (1997). https://doi.org/10.1063/1.366447
7. K. Toyota, S. Nakashima, T. Okada, Near-infrared laser-induced breakdown of liquid benzene. Chem. Phys. Lett. **323**, 323–328 (2000). https://doi.org/10.1016/S0009-2614(00)00532-7
8. J. Wang, H. Niino, A. Yabe, One-step microfabrication of fused silica by laser ablation of an organic solution. Appl. Phys. A **68**, 111–113 (1999). https://doi.org/10.1007/s003390050863
9. J. Ihlemann, B. Wolff-Rottke, Excimer laser micro machining of inorganic dielectrics. Appl. Surf. Sci. **106**, 282–286 (1996). https://doi.org/10.1016/S0169-4332(96)00422-9
10. J. Zhang, K. Sugioka, K. Midorikawa, High-speed machining of glass materials by laser-induced plasma-assisted ablation using a 532-nm laser. Appl. Phys. A **67**, 499–501 (1998). https://doi.org/10.1007/s003390050810
11. J. Zhang, K. Sugioka, K. Midorikawa, High-quality and high-efficiency machining of glass materials by laser-induced plasma-assisted ablation using conventional nanosecond UV, visible, and infrared lasers. Appl. Phys. A **69**, S876–S882 (1999). https://doi.org/10.1007/s003390051551
12. Y. Hanada, K. Sugioka, I. Miyamoto, K. Midorikawa, Double-pulse irradiation by laser-induced plasma-assisted ablation (LIPAA) and mechanisms study. Appl. Surf. Sci. **248**, 276–280 (2005). https://doi.org/10.1016/j.apsusc.2005.03.050
13. Y. Hanada, K. Sugioka, K. Obata, S. V. Garnov, I. Miyamoto, K. Midorikawa, Transient electron excitation in laser-induced plasma-assisted ablation of transparent materials, J. Appl. Phys. **99**, 043301 (2006). https://doi.org/10.1063/1.2171769
14. B. Hopp, T. Smausz, T. Csizmadia, C. Vass, T. Csákó, G. Szabó, Comparative study of different indirect laser-based methods developed for microprocessing of transparent materials. J. Laser Micro/Nanoeng. **5**, 80–85 (2010). https://doi.org/10.2961/jlmn.2010.01.0017
15. K. Zimmer, R. Böhme, B. Rauschenbach, Laser etching of fused silica using an adsorbed toluene layer. Appl. Phys. A **79**, 1883–1885 (2004). https://doi.org/10.1007/s00339-004-2961-y

16. B. Hopp, Cs. Vass, T. Smausz, Laser induced backside dry etching of transparent materials, Appl. Surf. Sci. **253**, 7922–7925 (2007). https://doi.org/10.1016/j.apsusc.2007.02.068
17. B. Hopp, T. Smausz, C. Vass, G. Szabó, R. Böhme, D. Hirsch, K. Zimmer, Laser-induced backside dry and wet etching of transparent materials using solid and molten tin as absorbers. Appl. Phys. A **94**, 899–904 (2009). https://doi.org/10.1007/s00339-009-5078-5
18. J. Wang, H. Niino, A. Yabe, Laser ablation of poly(methylmethacrylate) doped with aromatic compounds: Laser intensity dependence of absorption coefficient. Jpn. J. Appl. Phys. **38**, 871–876 (1999). https://doi.org/10.1143/JJAP.38.871
19. J. Ikeno, A. Kobayashi, T. Kasai, YAG laser processing of fused silica glass with the aid of solution, Jpn. Soc. Precis. Eng. **55**, 335–340 (1989) (in Japanese). https://doi.org/10.2493/jjspe.55.335
20. S.I. Dolgaev, A.A. Lyalin, A.V. Simakin, G.A. Shafeev, Etching of sapphire assisted by copper-vapour laser radiation. Quantum Electron. **26**, 65–68 (1996). https://doi.org/10.1070/QE1996v026n01ABEH000590
21. S.I. Dolgaev, A.A. Lyalin, A.V. Simakin, V.V. Voronov, G.A. Shafeev, Fast etching and metallization of via-holes in sapphire with the help of radiation by copper vapor laser. Appl. Surf. Sci. **109–110**, 201–205 (1997). https://doi.org/10.1016/S0169-4332(96)00660-5
22. M. Ehrhardt, P. Lorenz, B. Han, R. Zhu, K. Zimmer, Laser-induced backside wet etching of SiO_2 with a visible ultrashort laser pulse by using $KMnO_4$ solution as an absorber liquid. J. Laser Micro/Nanoeng. **13**, 47–54 (2018). https://doi.org/10.2961/jlmn.2018.02.0001
23. M. Y. Tsvetkov, V. I. Yusupov, N. V. Minaev, P. S. Timashev, K. M. Golant, V. N. Bagratashvili, Effects of thermo-plasmonics on laser-induced backside wet etching of silicate glass, Laser Phys. Lett. **13**, 106001 (2016). https://doi.org/10.1088/1612-2011/13/10/106001
24. O.M. Zhigalina, D.N. Khmelenin, A.V. Atanova, N.V. Minaev, A.P. Sviridov, M.Y. Tsvetkov, A nanoscale modification of materials at thermoplasmonic laser-induced backside wet etching of sapphire. Plasmonics **15**, 599–608 (2020). https://doi.org/10.1007/s11468-019-01091-9
25. H. F. Chang, W. K. Yeung, W. C. Kao, M. Ehrhardt, K. Zimmer, J. Y. Cheng, Surface micromachining on a polymethylmethacrylate substrate using visible laser-induced backside wet etching with a $KMnO_4$ solution as an absorber, J. Laser Appl. **32**, 022014 (2020). https://doi.org/10.2351/1.5114659
26. Z.Q. Huang, M.H. Hong, T.B.M. Do, Q.Y. Lin, Laser etching of glass substrates by 1064 nm laser irradiation. Appl. Phys. A **93**, 159–163 (2008). https://doi.org/10.1007/s00339-008-4674-0
27. X.Z. Xie, M.F. Hu, W.F. Chen, X. Wei, W. Hu, X.Y. Gao, X.R. Yuan, M.H. Hong, Cavitation bubble dynamics during laser wet etching of transparent sapphire substrates by 1064 nm laser irradiation. J. Laser Micro/Nanoeng. **8**, 259–265 (2013). https://doi.org/10.2961/jlmn.2013.03.0012
28. K.-K. Kwon, H. Kim, T. Kim, C. N. Chu, High aspect ratio channel fabrication with near-infrared laser-induced backside wet etching, J. Mater. Proc. Tech. **278**, 116505 (2020). https://doi.org/10.1016/j.jmatprotec.2019.116505
29. Cs. Vass, B. Hopp, T. Smausz, F. Ignácz, Experiments and numerical calculations for the interpretation of the backside wet etching of fused silica, Thin Solid Films **453–454** 121–126 (2004). https://doi.org/10.1016/j.tsf.2003.11.081
30. J. Wang, H. Niino, A. Yabe, Micromachining of quartz crystal with excimer lasers by laser-induced backside wet etching. Appl. Phys. A **69**, S271–S273 (1999). https://doi.org/10.1007/s003390051398
31. J. Wang, H. Niino, A. Yabe, Micromachining of transparent materials with super-heated liquid generated by multiphotonic absorption of organic molecule. Appl. Surf. Sci. **154–155**, 571–576 (2000). https://doi.org/10.1016/S0169-4332(99)00462-6
32. R. Böhme, A. Braun, K. Zimmer, Backside etching of UV-transparent materials at the interface to liquids. Appl. Surf. Sci. **186**, 276–281 (2002). https://doi.org/10.1016/S0169-4332(01)00630-4
33. K. Zimmer, R. Böhme, A. Braun, B. Rauschenbach, F. Bigl, Excimer laser-induced etching of sub-micron surface relief gratings in fused silica using phase grating projection. Appl. Phys. A **74**, 453–456 (2002). https://doi.org/10.1007/s003390101184

34. R. Böhme, K. Zimmer, Effect of halogenated organic solvents on laser-induced backside wet etching of fused silica. Appl. Phys. A **83**, 9–12 (2006). https://doi.org/10.1007/s00339-006-3483-6
35. H. Niino, Y. Yasui, X. Ding, A. Narazaki, T. Sato, Y. Kawaguchi, A. Yabe, Surface microfabrication of silica glass by excimer laser irradiation of organic solvent. J. Photochem. Photobiol. A: Chem. **158**, 179–182 (2003). https://doi.org/10.1016/S1010-6030(03)00032-7
36. X. Ding, T. Sato, Y. Kawaguchi, H. Niino, Laser-induced backside wet etching of sapphire. Jpn. J. Appl. Phys. **42**, L176–L178 (2003). https://doi.org/10.1143/JJAP.42.L176
37. K. Fujito, T. Hashimoto, K. Samonji, J.S. Speck, S. Nakamura, Growth of AlN by the chemical vapor reaction process and its application to lateral overgrowth on patterned sapphire substrates. J. Cryst. Growth **272**, 370–376 (2004). https://doi.org/10.1016/j.jcrysgro.2004.08.079
38. Cs. Vass, D. Sebők, B. Hopp, Comparing study of subpicosecond and nanosecond wet etching of fused silica, Appl. Surf. Sci. **252**, 4768–4772 (2006). https://doi.org/10.1016/j.apsusc.2005.07.118
39. X. Ding, Y. Yasui, Y. Kawaguchi, H. Niino, A. Yabe, Laser-induced back-side wet etching of fused silica with an aqueous solution containing organic molecules. Appl. Phys. A **75**, 437–440 (2002). https://doi.org/10.1007/s003390101131
40. X. Ding, Y. Kawaguchi, H. Niino, A. Yabe, Laser-induced high-quality etching of fused silica using a novel aqueous medium. Appl. Phys. A **75**, 641–645 (2002). https://doi.org/10.1007/s00339-002-1453-1
41. K. Zimmer, R. Böhme, D. Ruthe, B. Rauschenbach, Backside laser etching of fused silica using liquid gallium. Appl. Phys. A **84**, 455–458 (2006). https://doi.org/10.1007/s00339-006-3630-0
42. K. Zimmer, R. Böhme, D. Hirsch, B. Rauschenbach, Backside etching of fused silica with UV laser pulses using mercury. J. Phys. D: Appl. Phys. **39**, 4651–4655 (2006). https://doi.org/10.1088/0022-3727/39/21/022
43. J.Y. Cheng, M.H. Yen, C.W. Wei, Y.C. Chuang, T.H. Young, Crack-free direct-writing on glass using a low-power UV laser in the manufacture of a microfluidic chip. J. Micromech. Microeng. **15**, 1147–1156 (2005). https://doi.org/10.1088/0960-1317/15/6/005
44. H. Niino, Y. Kawaguchi, T. Sato, A. Narazaki, T. Gumpenberger, R. Kurosaki, Laser ablation of toluene liquid for surface micro-structuring of silica glass. Appl. Surf. Sci. **252**, 4387–4391 (2006). https://doi.org/10.1016/j.apsusc.2005.07.084
45. S. Pissadakis, R. Böhme, K. Zimmer, Sub-micron periodic structuring of sapphire by laser induced backside wet etching technique. Opt. Exp. **15**, 1428–1433 (2007). https://doi.org/10.1364/OE.15.001428
46. Cs. Vass, K. Osvay, Fabrication of 150 nm period grating in fused silica by two-beam interferometric laser induced backside wet etching method, Opt. Exp. **14**, 8354–8359 (2006). https://doi.org/10.1364/OE.14.008354
47. B. Kiss, F. Ujhelyi, Á. Sipos, B. Farkas, P. Dombi, K. Osvay, C. Vass, Microstructuring of transparent dielectric films by twin-LIBWE method for OWLS applications. J. Laser Micro/Nanoeng. **8**, 271–275 (2013). https://doi.org/10.2961/jlmn.2013.03.0014
48. C. Vass, B. Kiss, R. Flender, Z. Felházi, P. Lorenz, M. Ehrhardt, K. Zimmer, Comparative study on grating fabrication in transparent materials by TWIN-LIBWE and ultrashort pulsed ablation techniques. J. Laser Micro/Nanoeng. **10**, 38–42 (2015). https://doi.org/10.2961/jlmn.2015.01.0008
49. J. Wang, H. Niino, A. Yabe, Microfabrication of a fluoropolymer film using conventional XeCl excimer laser by laser-induced backside wet etching. Jpn. J. Appl. Phys. **38**, L761–L763 (1999). https://doi.org/10.1143/JJAP.38.L761
50. G. Kopitkovas, T. Lippert, N. Murazawa, C. David, A. Wokaun, J. Gobrecht, R. Winfield, Laser processing of micro-optical components in quartz. Appl. Surf. Sci. **254**, 1073–1078 (2007). https://doi.org/10.1016/j.apsusc.2007.09.048
51. Y. Yasui, H. Niino, Y. Kawaguchi, A. Yabe, Microetching of fused silica by laser ablation of organic solution with XeCl excimer laser. Appl. Surf. Sci. **186**, 552–555 (2002). https://doi.org/10.1016/S0169-4332(01)00635-3

52. G. Kopitkovas, T. Lippert, C. David, A. Wokaun, J. Gobrecht, Fabrication of micro-optical elements in quartz by laser induced backside wet etching. Microelectron. Eng. **67–68**, 438–444 (2003). https://doi.org/10.1016/S0167-9317(03)00099-6
53. G. Kopitkovas, T. Lippert, C. David, A. Wokaun, J. Gobrecht, Surface micromachining of UV transparent materials. Thin Solid Films **453–454**, 31–35 (2004). https://doi.org/10.1016/j.tsf.2003.11.074
54. K. Zimmer, A. Braun, R. Böhme, Etching of fused silica and glass with excimer laser at 351 nm. Appl. Surf. Sci. **208–209**, 199–204 (2003). https://doi.org/10.1016/S0169-4332(02)01372-7
55. Z.Q. Huang, M.H. Hong, K.S. Tiaw, Q.Y. Lin, Quality glass processing by laser induced backside wet etching. J. Laser Micro/Nanoeng. **2**, 194–199 (2007). https://doi.org/10.2961/jlmn.2007.03.0006
56. M. Ehrhardt, G. Raciukaitis, P. Gecys, K. Zimmer, Microstructuring of fused silica by laser-induced backside wet etching using picosecond laser pulses. Appl. Surf. Sci. **256**, 7222–7227 (2010). https://doi.org/10.1016/j.apsusc.2010.05.055
57. M. Ehrhardt, G. Raciukaitis, P. Gecys, K. Zimmer, Laser-induced backside wet etching of fluoride and sapphire using picosecond laser pulses. Appl. Phys. A **101**, 399–404 (2010). https://doi.org/10.1007/s00339-010-5833-7
58. M.Y. Tsvetkov, V.I. Yusupov, P.S. Timashev, K.M. Golant, N.V. Minaev, S.I. Tsypina, V.N. Bagratashvili, On the role of supercritical water in laser-induced backside wet etching of glass. Russ. J. Phys. Chem. B **11**, 1061–1069 (2017). https://doi.org/10.1134/S1990793117070181
59. J.Y. Cheng, M.H. Yen, T.H. Young, Crack-free micromachining on glass using an economic Q-switched 532 nm laser. J. Micromech. Microeng. **16**, 2420–2424 (2006). https://doi.org/10.1088/0960-1317/16/11/024
60. J.Y. Cheng, M.H. Yen, W.C. Hsu, J.H. Jhang, T.H. Young, ITO patterning by a low power Q-switched green laser and its use in the fabrication of a transparent flow meter. J. Micromech. Microeng. **17**, 2316–2323 (2007). https://doi.org/10.1088/0960-1317/17/11/019
61. T. Sato, Y. Kawaguchi, R. Kurosaki, A. Narazaki, W. Watanabe, H. Niino, Laser-induced backside wet etching employing green DPSS laser and liquid metallic absorber. J. Laser Micro/Nanoeng. **6**, 204–208 (2011). https://doi.org/10.2961/jlmn.2011.03.0006
62. J. Y. Cheng, M. Z. Mousavi, C. Y. Wu, H. F. Tsai, Blue light emission from a glass/liquid interface for real-time monitoring of a laser-induced etching process, J. Micromech. Microeng. **21**, 075019 (2011). https://doi.org/10.1088/0960-1317/21/7/075019
63. T. Nakazumi, T. Sato, A. Narazaki, H. Niino, Laser marking on soda-lime glass by laser-induced backside wet etching with two-beam interference, J. Micromech. Microeng. **26**, 095015 (2016). https://doi.org/10.1088/0960-1317/26/9/095015
64. M.H. Yen, C.W. Huang, W.C. Hsu, T.H. Young, K. Zimmer, J.Y. Cheng, Crack-free micromachining on glass substrates by visible LIBWE using liquid metallic absorbers. Appl. Surf. Sci. **257**, 87–92 (2010). https://doi.org/10.1016/j.apsusc.2010.06.041
65. Cs. Vass, B. Kiss, J. Kopniczky, B. Hopp, Etching of fused silica fiber by metallic laser-induced backside wet etching technique, Appl. Surf. Sci. **278**, 241–244 (2013). https://doi.org/10.1016/j.apsusc.2012.11.163
66. J.Y. Cheng, H.Y. Chen, M.Z. Mousavi, C.Y.Y. Chang, Crack-free micromachining of glass ceramic using visible LIBWE. J. Laser Micro/Nanoeng. **8**, 253–258 (2013). https://doi.org/10.2961/jlmn.2013.03.0011
67. J.Y. Cheng, W.C. Kao, M.Z. Mousavi, H.F. Chang, W.C. Hsu, M.H. Yen, M. Ehrhardt, K. Zimmer, High-quality surface micromachining on polymer using visible-LIBWE. J. Laser Micro/Nanoeng. **11**, 117–123 (2016). https://doi.org/10.2961/jlmn.2016.01.0022
68. K. Zimmer, R. Böhme, S. Pissadakis, L. Hartwig, G. Reisse, B. Rauschenbach, Backside etching of fused silica with Nd:YAG laser. Appl. Surf. Sci. **253**, 2796–2800 (2006). https://doi.org/10.1016/j.apsusc.2006.05.059
69. X. Zhao, M. Ehrhardt, P. Lorenz, B. Han, K. Zimmer, L. Xu, X. Ni, Nanosecond Nd:YAG laser induced backside wet etching of NaCl with eutectic gallium-indium alloy as absorbing liquid, Surf. Interfaces **17**, 100353 (2019). https://doi.org/10.1016/j.surfin.2019.100353

70. G. Kopitkovas, T. Lippert, C. David, S. Canulescu, A. Wokaun, J. Gobrecht, Fabrication of beam homogenizers in quartz by laser micromachining. J. Photochem. Photobiol. A: Chem. **166**, 135–140 (2004). https://doi.org/10.1016/j.jphotochem.2004.05.001
71. K. Zimmer, R. Böhme, Precise etching of fused silica for micro-optical applications. Appl. Surf. Sci. **243**, 415–420 (2005). https://doi.org/10.1016/j.apsusc.2004.09.118
72. T. Sato, Y. Kawaguchi, T. Kurosaki, A. Narazaki, W. Watanabe, H. Niino, Variation in the etch rate of LIBWE fabricating deep microtrenches. J. Laser Micro/Nanoeng. **7**, 81–86 (2012). https://doi.org/10.2961/jlmn.2012.01.0016
73. Y. Kawaguchi, T. Sato, A. Narazaki, R. Kurosaki, H. Niino, Etching a micro-trench with a maximum aspect ratio of 60 on silica glass by laser-induced backside wet etching (LIBWE). Jpn. J. Appl. Phys. **44**, L176–L178 (2005). https://doi.org/10.1143/JJAP.44.L176
74. Y. Kawaguchi, T. Sato, A. Narazaki, R. Kurosaki, H. Niino, Rapid prototyping of silica glass microstructures by the LIBWE method: Fabrication of deep microtrenches. J. Photochem. Photobiol. A: Chem. **182**, 319–324 (2006). https://doi.org/10.1016/j.jphotochem.2006.05.033
75. T. Sato, R. Kurosaki, A. Narazaki, Y. Kawaguchi, H. Niino, Flexible 3D deep microstructures of silica glass by laser-induced backside wet etching. Appl. Phys. A **101**, 319–323 (2010). https://doi.org/10.1007/s00339-010-5790-1
76. T. Sato, R. Kurosaki, Y. Kawaguchi, A. Narazaki, H. Niino, Fabrication of multiple slanted microstructures on silica glass by laser-induced backside wet etching. J. Laser Micro/Nanoeng. **5**, 256–262 (2010). https://doi.org/10.2961/jlmn.2010.03.0014
77. T. Sato, R. Kurosaki, A. Narazaki, Y. Kawaguchi, H. Niino, Flexible fabrication of deep microstructures by laser-induced backside wet etching, Proc. SPIE **7584**, 758408 (2010). https://doi.org/10.1117/12.841583
78. C. Vass, K. Osvay, B. Hopp, Z. Bor, 104 nm period grating fabrication in fused silica by immersion two-beam interferometric laser induced backside wet etching technique. Appl. Phys. A **87**, 611–613 (2007). https://doi.org/10.1007/s00339-007-3891-2
79. Cs. Vass, K. Osvay, M. Csete, B. Hopp, Fabrication of 550 nm gratings in fused silica by laser induced backside wet etching technique, Appl. Surf. Sci. **253**, 8059–8063 (2007). https://doi.org/10.1016/j.apsusc.2007.02.087
80. C. Vass, K. Osvay, T. Véső, B. Hopp, Z. Bor, Submicrometer grating fabrication in fused silica by interferometric laser-induced backside wet etching technique. Appl. Phys. A **93**, 69–73 (2008). https://doi.org/10.1007/s00339-008-4636-6
81. B. Kiss, Cs. Vass, P. Heck, P. Dombi, K. Osvay, Fabrication and analysis of transmission gratings produced by the indirect laser etching technique, J. Phys. D: Appl. Phys. **44**, 415103 (2011). https://doi.org/10.1088/0022-3727/44/41/415103
82. C.B. Arnold, A. Piqué, Laser Direct-Write Processing. MRS Bull. **32**, 9–11 (2007). https://doi.org/10.1557/mrs2007.9
83. H. Niino, Y. Kawaguchi, T. Sato, A. Narazaki, R. Kurosaki, Surface microstructuring of silica glass by laser-induced backside wet etching with a DPSS UV laser. Appl. Surf. Sci. **253**, 8287–8291 (2007). https://doi.org/10.1016/j.apsusc.2007.02.099
84. T. Sato, A. Narazaki, H. Niino, Fabrication of micropits by LIBWE for laser marking of glass materials. J. Laser Micro/Nanoeng. **12**, 248–253 (2017). https://doi.org/10.2961/jlmn.2017.03.0013
85. H. Fukumura, H. Masuhara, The mechanism of dopant-induced laser ablation. Possibility of cyclic multiphotonic absorption in excited states, Chem. Phys. Lett. **221**, 373–378 (1994). https://doi.org/10.1016/0009-2614(94)00277-0
86. Cs. Vass, T. Smausz, B. Hopp, Wet etching of fused silica: a multiplex study, J. Phys. D: Appl. Phys. **37**, 2449–2454 (2004). https://doi.org/10.1088/0022-3727/37/17/018
87. K. Zimmer, Analytical solution of the laser-induced temperature distribution across internal material interfaces. Int. J. Heat Mass Trans. **52**, 497–503 (2009). https://doi.org/10.1016/j.ijheatmasstransfer.2008.03.034
88. R. Böhme, K. Zimmer, The influence of the laser spot size and the pulse number on laser-induced backside wet etching. Appl. Surf. Sci. **247**, 256–261 (2005). https://doi.org/10.1016/j.apsusc.2005.01.058

89. M.Y. Tsvetkov, V.I. Yusupov, N.V. Minaev, A.A. Akovantseva, P.S. Timashev, K.M. Golant, B.N. Chichkov, V.N. Bagratashvili, On the mechanisms of single-pulse laser-induced backside wet etching. Opt. Laser Technol. **88**, 17–23 (2017) https://doi.org/10.1016/j.optlastec.2016.05.020
90. R. Böhme, D. Spemann, K. Zimmer, Surface characterization of backside-etched transparent dielectrics. Thin Solid Films **453–454**, 127–132 (2004). https://doi.org/10.1016/j.tsf.2003.11.083
91. G. Kopitkovas, V. Deckert, T. Lippert, F. Raimondi, C.W. Schneider, A. Wokaun, Chemical and structural changes of quartz surfaces due to structuring by laser-induced backside wet etching. Phys. Chem. Chem. Phys. **10**, 3195–3202 (2008). https://doi.org/10.1039/B800090E
92. C. Vass, J. Budai, Z. Schay, B. Hopp, Interpretation and modeling of laser-induced backside wet etching procedure. J. Laser Micro/Nanoeng. **5**, 43–47 (2010). https://doi.org/10.2961/jlmn.2010.01.0010
93. K. Zimmer, M. Ehrhardt, R. Böhme, Simulation of laser-induced backside wet etching of fused silica with hydrocarbon liquids, J. Appl. Phys. **107**, 034908 (2010). https://doi.org/10.1063/1.3276204
94. K. Zimmer, R. Böhme, M. Ehrhardt, B. Rauschenbach, Mechanism of backside etching of transparent materials with nanosecond UV-lasers. Appl. Phys. A **101**, 405–410 (2010). https://doi.org/10.1007/s00339-010-5878-7
95. T. Lee, D. Jang, D. Ahn, D. Kim, Effect of liquid environment on laser-induced backside wet etching of fused silica, J. Appl. Phys. **107**, 033112 (2010). https://doi.org/10.1063/1.3294615
96. Y. Kawaguchi, X. Ding, A. Narazaki, T. Sato, H. Niino, Transient pressure induced by laser ablation of liquid toluene: toward the understanding of laser-induced backside wet etching. Appl. Phys. A **79**, 883–885 (2004). https://doi.org/10.1007/s00339-004-2580-7
97. Y. Kawaguchi, X. Ding, A. Narazaki, T. Sato, H. Niino, Transient pressure induced by laser ablation of toluene, a highly laser-absorbing liquid. Appl. Phys. A **80**, 275–281 (2005). https://doi.org/10.1007/s00339-003-2347-6
98. R. Böhme, T. Otto, K. Zimmer, In situ reflectivity investigations of solid/liquid interface during laser backside etching. Appl. Surf. Sci. **252**, 4392–4396 (2006). https://doi.org/10.1016/j.apsusc.2005.06.044
99. A. Vogel, R. Engelhardt, U. Behnle, U. Parlitz, Minimization of cavitation effects in pulsed laser ablation illustrated on laser angioplasty. Appl. Phys. B **62**, 173–182 (1996). https://doi.org/10.1007/BF01081122
100. X. Ding, Y. Kawaguchi, T. Sato, A. Narazaki, H. Niino, Site-selective dye deposition on microstructures of fused silica fabricated using the LIBWE method, Chem. Commun. 2168–2169 (2003). https://doi.org/10.1039/B306770J
101. X. Ding, Y. Kawaguchi, T. Sato, A. Narazaki, H. Niino, Fabrication of microarrays on fused silica plates using the laser-induced backside wet etching method. Langmuir **20**, 9769–9774 (2004). https://doi.org/10.1021/la0498004
102. P. Karásek, J. Grym, M. Roth, J. Planeta, F. Foret, Etching of glass microchips with supercritical water. Lab Chip **15**, 311–318 (2015). https://doi.org/10.1039/C4LC00843J
103. J.Y. Cheng, M.Z. Mousavi, C.Y. Wu, H.F. Tsai, Blue light plasma emission during LIBWE using 532 nm Q-switched nanosecond laser. J. Laser Micro/Nanoeng. **7**, 87–92 (2012). https://doi.org/10.2961/jlmn.2012.01.0017